

Ferromagnetic Impurity Induced Majorana Zero Mode in Iron-Based Superconductor

Rui Song,^{1,2,3} Ping Zhang,^{4,2,5,*} Xian-Tu He,^{2,5} and Ning Hao^{3,†}

¹*HEDPS, Center for Applied Physics and Technology and School of Physics, Peking University, Beijing 100871, China*

²*HEDPS, Center for Applied Physics and Technology and School of Engineering, Peking University, Beijing 100871, China*

³*Anhui Key Laboratory of Condensed Matter Physics at Extreme Conditions,
High Magnetic Field Laboratory, HFIPS, Anhui, Chinese Academy of Sciences,
and University of Science and Technology of China, Hefei, China*

⁴*School of Physics and Physical Engineering, Qufu Normal University, Qufu 273165, China*

⁵*Institute of Applied Physics and Computational Mathematics, Beijing 100088, China*

Recent experiments reported the puzzling zero energy modes associated with ferromagnetic impurities in some iron-based superconductors with topological band structures. Here, we show that the sufficiently strong exchange coupling between a ferromagnetic impurity and substrate can trigger a quantum phase transition, beyond which, the phase of the superconducting order parameter around the impurity acquires a sign-change. In such a case, we prove that a Majorana mode can be induced and trapped by the impurity in the superconducting state of the electrons from the topological bands with linear dispersion. Furthermore, we show that our theory can explain the controversial observations and confusing features of the zero energy modes from recent experiments in some iron-based superconductors.

In superconductor, the impurity can induce various quasi-particle states, such as Yu-Shiba-Rusinov (YSR) state from the classical impurity scattering potential[1-3] and Kondo resonance state from the impurity in quantum limit[4]. Through elucidating their properties, one can obtain a lot of critical information on electron pairing[5]. Meanwhile, the quasi-particle state itself can manifest some unexpected behaviors. In particular, an interstitial iron impurity (IFI) induced robust zero-energy mode has been reported by the scanning tunnelling microscopy/spectroscopy (STM/S) in iron-based superconductor Fe(Te,Se)[6]. The subsequent studies have been extended to other iron-based superconductors such as monolayer Fe(Te,Se)/SrTiO₃ and LiFeAs, and the similar zero-energy mode is also observed[7, 8]. Experimentally, the zero-energy mode can only be observed on partial iron impurities and is robust against the external magnetic field, and the critical temperature is much below the superconducting transition temperature T_c . Besides, these materials share a remarkable feature of possessing topological bands, which implies the zero-energy mode could be Majorana mode. On the contrary, some revisited studies on Fe(Te,Se) claim the observed zero-energy mode is just trivial YSR states with near-zero-energy electron-like and hole-like components[9, 10]. Thus, the understandings of the properties and the mechanism of the zero-energy mode in these iron-based superconductors are still in debate[6-12].

In this work, we first perform the first-principles calculations to investigate the interaction between the IFI and the substrate FeSe_{0.45}Te_{0.55}. The numerical results indicate the exchange coupling $J(\mathbf{r}, z)$ between the magnetic moment of IFI and the spin of the 3d electron of FeSe_{0.45}Te_{0.55} has the form of Friedel-like oscillation with the characteristic length a_0 , which is the lattice constant of iron square lattice. The amplitude of $J(\mathbf{r}, z)$ and the

magnetic moment of IFI strongly depend on the height z between IFI and substrate. Based on the information, we further consider the impact of the IFI on the local superconducting order parameter $\Delta(\mathbf{r})$ by solving the Bogoliubov-de Gennes (BdG) equations on the iron square lattice with self-consistency. We find that there exists a quantum phase transition at a critical height z_c , *i.e.* a critical $J_c(\mathbf{r}, z_c)$, beyond which, $\Delta(\mathbf{r})$ change sign in the regime with $r < a_0$. Note that the surface states dominate the STM/S measurements. Accordingly, the topological surface bands acquire the superconducting pairing with the same configuration of $\Delta(\mathbf{r})$. In such a case, we prove that a Majorana zero mode can be induced by the IFI due to the topological surface bands. For the smaller $J(\mathbf{r}, z) < J_c(\mathbf{r}, z_c)$, the quantum phase transition cannot be triggered. The IFI can only induce the trivial YSR states of the projected bulk bands, which has the near-zero energy in vicinity of quantum phase transition. Within this picture, the contradictions between the results from different STM/S measurements can be solved, and the properties of the zero-energy mode, such as the robustness against external magnetic field and lower critical temperature can also be understood.

The STM experiment shows that the height of IFI can be tuned by the STM tip[8, 10]. During the process of the approaching, the transition from the YSR state to zero-energy mode happens[8]. It indicates that the coupling between the IFI and the substrate play a crucial role to observe the zero-energy mode. To elucidate the properties of such coupling, we construct a 9×9×1 supercell including a substrate Fe(Te,Se) with a suspended IFI. The calculation details are present in supplementary materials (SMs). Here, we only summarize the main results in Fig. 1. From Fig. 1 (a), one can find that the there exists a strong charge transfer between the IFI and the nearest neighbor substrate iron atoms, and such transfer

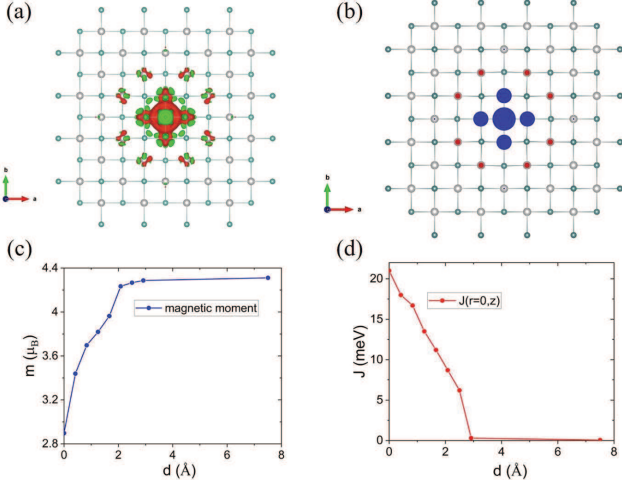


FIG. 1: (a) The spacial distributions of differential charge density of a supercell involving a $9 \times 9 \times 1$ Fe(Te,Se) substrate and a suspended IFI. (b) The spacial distributions of the induced spin polarizations of the 3d electrons of iron atoms in the substrate. The size and color of the dots denote the strength and direction of the spin polarization, respectively. (c)-(d) The magnetic moment of IFI and the effective exchange coupling $J(r = 0, z)$ as a function of the height d between the IFI and the substrate, respectively.

decays abruptly as expected. The calculated spin polarizations of substrate iron atoms shown in Fig. 1 (b) indicate the exchange coupling $J(\mathbf{r}, z_0)$ has the form of Friedel-like oscillation, which is consistent with the neutron scattering experiment on the Fe(Te,Se) with higher concentration of Te[13]. The characteristic length measured oscillation period is about the lattice constant a_0 from the Fig. 1 (b). The findings are further supported by the magnetic moment of IFI as a function of height, as shown in Fig. 1 (c). As the IFI approaches the substrate, the magnetic moment of IFI is suppressed. It indicates the spin transfer also happens and the exchange coupling between the magnetic moment of IFI and the 3d electrons of substrate Fe is strong. The strength of the exchange coupling $J(\mathbf{r} = 0, z_0)$ can be roughly estimated and is shown in Fig. 1 (d) (See SMs for details).

With above information, we extract a simplified model defined on a square lattice to evaluate the impact of the IFI to the local superconducting state of the Fe(Te,Se) substrate. The model Hamiltonian has the form,

$$H_{eff} = H_{BdG} + H_{coup}. \quad (1)$$

Here, the superconducting BdG Hamiltonian H_{BdG} and the coupling H_{coup} between the impurity and the sub-

strate has the following forms,

$$H_{BdG} = \sum_{\langle i,j \rangle} (t_{ij} - \mu \delta_{ij}) c_i^\dagger c_j + \sum_{i,j} \Delta_{ij} (c_{i\uparrow}^\dagger c_{j\downarrow}^\dagger + c.c.), \quad (2)$$

$$H_{coup} = \int d\mathbf{r} J(\mathbf{r}, z_0) \mathbf{S}_{imp} \cdot \boldsymbol{\sigma}. \quad (3)$$

Here, the first term in Eq. (2) describes the projected bulk hole-type band near surface Brillouin zone center. t_{ij} takes nonzero value t for the only nearest-neighbor hoppings. μ is the chemical potential. Δ_{ij} is the site-dependent superconducting order parameter which only involves the on-site term without loss of generality. \mathbf{S}_{imp} and $\boldsymbol{\sigma}$ in Eq. (3) label the magnetic moment of the IFI and the spin of 3d electron of substrate iron atoms, respectively. Here, we only consider the spin polarization along z direction. $J(\mathbf{r}, z_0)$ plays important role only in the first oscillating period a_0 which only involves the on-site and the nearest-neighbor iron atoms. The nearest-neighbor $J(\mathbf{r}, z_0)$ is less than J_c according to Fig. 1. Here, we consider the on-site term $J(\mathbf{r} = 0, z_0)$ for simplicity. The numeric details are present in SMs. As exchange coupling $J(\mathbf{r} = 0, z_0)$ increases from zero, there exists a quantum phase transition[5, 14, 15] at a critical $J_c \sim 1.2t$, beyond which, the local superconducting order parameter suddenly changes sign and becomes negative, as shown in Fig. 2 (b). Meanwhile, the level cross of two components of YSR states happens, as shown in Fig. 2 (a). In such a case, the spacial distributions of $\Delta(r)$ shown in Fig. 2 (c) indicate that $\Delta(r)$ acquires a π phase difference in the regime with $r < R_0$ in comparison with the one in the regime with $r > R_0$. Note that R_0 can take the value of lattice constant a_0 , when the nearest-neighbor term of $J(\mathbf{r}, z_0)$ is involved (See the SMs for details). This is a very crucial result from the effect of the IFI[14–18]. Though the quantum phase transition is not driven by temperature, the increase of temperature could quench it, thereafter, we calculate the critical temperature of the quantum phase transition T_q and find that T_q is quite lower than the bulk superconducting transition temperature T_c . We will return to this temperature effect when we connect our theory to the experiment below.

Now, we consider the effect of the spacial variation of the $\Delta(r)$ to the topological surface states. According to the theory of the topological superconductivity in iron-based superconductors[19–23], the electrons of topological surface band are paired in spin-singlet channel from the inter-band scattering or intrinsic proximity effect between the surface band and the projected bulk bands. As a result, the superconducting order parameter of topological surface band $\Delta_s(r)$ should have the same spacial configuration of the projected bulk bands $\Delta(r)$. In such a case, the effective Hamiltonian describing the topological surface superconductivity has the following form,

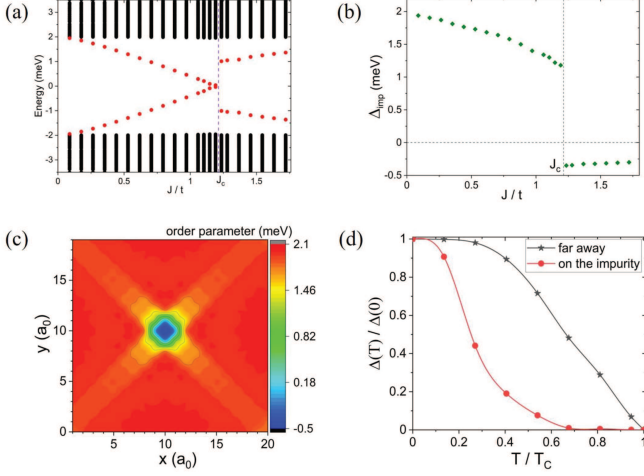


FIG. 2: (a) The energy spectrum as a function of exchange coupling $J(r = 0, z)$ from the self-consistent solution of Eq. (1). The red dots with opposite energy are a pair of YSR states. (b) The order parameter of superconducting state $\Delta(r = 0)$ as a function of exchange coupling $J(r = 0, z)$ from the self-consistent solution of Eq. (1). (c) The spacial distributions of $\Delta(r)$ under the condition $J(r = 0, z) = 1.2t$. (d) The temperature evolution of the $\Delta(r)$ from the self-consistent solution of Eq. (1).

$$H_s = [v_F(\mathbf{k} \times \boldsymbol{\sigma}) \cdot \hat{\mathbf{z}} - \mu] \tau_z + \Delta_s(r) \tau_x. \quad (4)$$

Here, H_s is spanned in the Nambu space, *i.e.*, $[c_\uparrow, c_\downarrow, c_\downarrow^\dagger, -c_\uparrow^\dagger]$. $\tau_{x/z}$ is the Pauli matrix to span the particle-hole space. $\Delta_s(r) = -\Delta_1$ when $r < R_0$ and $\Delta_s(r) = \Delta_2$ when $r > R_0$. Note that $\Delta_{1/2} > 0$ and $\Delta_1 \ll \Delta_2$. The phase of $\Delta_{1/2}$ is uniform and is omitted here, because there is not topological defect such as vortex. Thus, $\Delta_{1/2}$ is angle-independent and $\Delta_s(r)$ can only take real value in Eq. (4). In continuum limit, the eigen-equation of H_s is

$$H_s(\mathbf{k} \rightarrow -i\nabla) \psi(r, \theta) = E \psi(r, \theta), \quad (5)$$

which can be solved under aforementioned boundary conditions with a disk configuration, as shown in Fig.3 (a). The emergence of Majorana zero mode requires one can find a bound-state solution with $E = 0$ and whose wave-function satisfies $\mathcal{C}\psi = \eta\psi$ with $\mathcal{C} = i\sigma_y\tau_y K$ the particle-hole symmetry operator and $\eta = \pm 1$. Indeed, this kind of solution exists. We first give a simple picture to understand its existence. It is well known that the $0 - \pi$ topological surface superconducting junction can support the one-dimensional linear-dispersion Majorana mode[24, 25], as shown in Fig. 3 (a). The disk can be formed by bending the $0 - \pi$ junction to connect two ends. In such a case,

the one-dimensional linear-dispersion Majorana mode has to split into series quantized states labeled by the quantum numbers of the angular momentum, among which, a zero-energy bound state has to emerge, which is the Majorana zero-energy mode. Note that the wave function $\psi(r, \theta)$ has to obey the antiperiodic boundary conditions, $\psi(r, \theta) = -\psi(r, \theta + 2\pi)$ as pointed out by Fu *et al*[24]. The details of the analytic and numerical solution are shown in SMs. Here, we only discuss the main results. For the boundless disk, the wave function of Majorana zero mode takes the form $\psi_M(r, \theta) = [e^{-i\theta/2}u_\uparrow(r), e^{i\theta/2}u_\downarrow(r), e^{-i\theta/2}v_\downarrow(r), -e^{i\theta/2}v_\uparrow(r)]$ with the condition $u_\sigma(r) = -v_\sigma(r)$. $u_\sigma(r) = a_\sigma J_{\pm 1/2}(k_F r)e^{r/\xi_1}$ for $r < R_0$ and $u_\sigma(r) = b_\sigma J_{\pm 1/2}(k_F r)e^{-r/\xi_2}$ for $r > R_0$. $J_{\pm 1/2}(k_F r)$ is the Bessel functions with $\pm 1/2$ for spin up and down, respectively. a_σ and b_σ are the coefficients, which are determined by the continuity and normalization of wave function. Fermi wave vector $k_F = \mu/v_F$. Decay length $\xi_{1/2} = v_F/\Delta_{1/2}$. The STS measured differential conductance $dI/dV \propto \sum_\sigma r|u_\sigma(r)|^2\delta(\omega - eV) + |v_\sigma(r)|^2\delta(\omega + eV)$. The case of Majorana zero mode is plotted in Fig.3 (b), from which, one can find that the spacial profile of dI/dV is consistent with the observation in monolayer Fe(Te,Se)/SrTiO₃[7] but has subtle difference near $r = 0$ in comparison with the measurements in bulk Fe(Te,Se) and LiFeAs[6, 8]. We argue this tiny difference is from the effect of the IFI, such as the mixture of the electronic state, electron's inelastic tunneling process or finite quasi-particle scattering etc. In Fig. 3 (c), we consider the modulation from the finite quasi-particle scattering and the resulting spectrum is quite similar to the cases in bulk Fe(Te,Se) and LiFeAs. For the finite disk, the numerical results are also consistent with the analytic solutions (See SMs for details).

The aforementioned theory can be utilized to understand the multiple features and common properties of the zero-energy modes in iron-based superconductors. We summarize the bound-state spectrum as function as exchange coupling $J(\mathbf{r} = 0, z_0)$ in Fig. 3 (b). One can find that there exists a pair of near-zero-energy YSR states from the projected bulk bands when $J(\mathbf{r} = 0, z_0)$ is close to J_c . The electron-like and hole-like components of a pair of near-zero-energy YSR states has opposite spin polarizations. Thus, the whole of them shows no spin-resolved feature. When $J(\mathbf{r} = 0, z_0)$ is larger than J_c , a pair of near-zero-energy YSR states steeply split, and the robust Majorana zero mode emerge from the topological surface bands. Thus, we argue that the contradictions from different STM/S experiments root in the selected IFIs with different exchange couplings $J(\mathbf{r} = 0, z)$, which coincides with the fact that the zero energy modes can be only observed on a partial IFIs[6–8]. The fragileness of the near-zero-energy YSR state and the robustness of the Majorana zero mode against the external magnetic

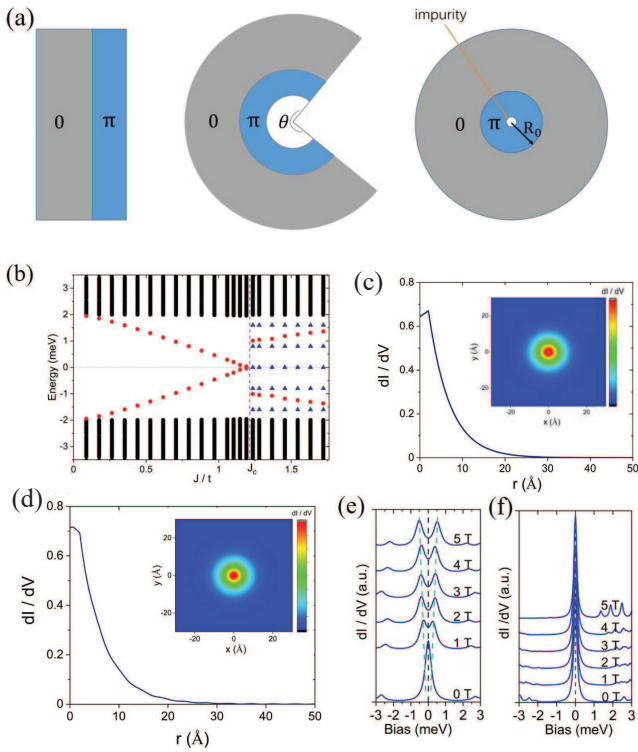


FIG. 3: (a) The schematic plotting to show the $0 - \pi$ junction bends to form a disk. (b) The overall energy spectrum from the projected bulk bands labelled by black and red colors, and from the topological surface bands labelled by the blue color. The former is the same as Fig. 1, and the latter is from the numerical solution of Eq. (4) defined in the finite disk configuration. (c) The simulated dI/dV profile for the Majorana zero mode from the analytic solutions of Eq. (4) defined in the boundless disk configuration. (d) The simulated dI/dV profile for the Majorana zero mode by take into account the quasi-particle scattering. The inset in (c) and (d) are the simulated dI/dV two-dimensional spacial profiles. (e) and (f) The external magnetic field effect to the YSR states and the Majorana zero mode, respectively.

field can also be understood. We consider the Zeeman energy m_z of the external magnetic field. For a pair of near-zero-energy YSR states, the opposite spin polarization indicates they have to split according to $m_z \sigma_z$ under external magnetic field, as shown in Fig. 3 (e). For the Majorana zero mode, the Zeeman term can be added into H_s in Eq. (4) with the effect to open a gap to the Dirac bands. We find that the solution form of Majorana zero mode is not changed but with a modulated $k'_F = \sqrt{\mu^2 - m_z^2}/v_F$. Thus, the Majorana zero mode is robust under the condition $m_z < \mu$. Note that H_s plus $m_z \sigma_z$ is also one copy of decoupled Hamiltonian to describe the case in monolayer $\text{Fe}(\text{Te},\text{Se})/\text{SrTiO}_3$ [7], in which the two-dimensional Dirac bands are from the bulk. Some experiments have observed that the Majorana zero mode disappears at a temperature below T_c [6–

8]. This behavior can also be understood from the self-consistent calculation results, as shown in Fig. 2 (d). One can find that the sign-change $\Delta_s(r = 0)$ decays to zero at about $T_q \sim 0.6T_c$. We argue this is the primary reason for the temperature effect in spite of the possible quasi-particle poisoning[26, 27]. It is worth noting that the magnetic impurity induced robust energy mode has also been observed in PbTaSe_2 [28], which has topological band structure and is superconducting. Within our theory, the observations in PbTaSe_2 can be well understood.

At last, the reliability of the theory can be enhanced by estimating some relevant parameters. The first one is critical exchange coupling $J_c \sim 1.2t$. t measures the energy scale of the projected bulk bands. It has no exact value, because it reflects the average effect involving the bands across $\Gamma - Z$ line. According to estimation, it can take about 10 meV. Then, $J_c \sim 12$ meV. Note that the aforementioned calculations do not involve the correlated interaction effect, which can further reduce the band width measured by t [29]. Besides, the atomic spin-orbital coupling can further reduce the value of the critical $J(\mathbf{r} = 0, z)$ to trigger the quantum phase transition. Thus, the required J_c should be much smaller than 12 meV. The IFI can have a magnetic moment $m \sim 5\mu_B$, which can induce a magnetic dipole field $B(r) = \mu_0 m / 4\pi r^3$ [30, 31]. The induced magnetic flux can be calculated by setting the lower limit of integral cut-off to be the Wigner-Seitz radius of the iron atom. If one quantized magnetic vortex emerges, it requires the magnetic moment to extend to be $10^4\mu_B$, which is only possible for a magnetic cluster in nanoscale.

In conclusion, we provide a new understanding to resolve the debate about whether the STM/S observed zero energy mode induced by interstitial iron impurity on some iron-based superconductors is Majorana zero mode or not. We find that a quantum phase transition can be triggered by the exchange coupling between the interstitial iron impurity and iron-based superconductor substrate. In such a case, the local superconducting order parameter changes sign around the impurity, and we prove that a robust Majorana zero mode can be induced and trapped by the impurity through taking into account the topological surface bands. Our theory can explain series confusing features observed by the experiments. More meaningfully, our theory can be extended to other material categories, which host both topological bands and superconductivity.

N. Hao thanks J. P. Hu, X. X. Wu, S. B. Zhang, S. S. Qin, F. W. Zheng, H. F. Du, L. Shan, Z. Y. Wang, S. C. Yan and X. Y. Hou for helpful discussions. This work was financially supported by the National Key R&D Program of China No. 2017YFA0303201, National Natural Science Foundation of China under Grants (No. 12022413, No. 11674331, No. 11625415), the “Strategic Priority Research Program (B)” of the Chinese Academy of Sciences, Grant No. XDB33030100, the ‘100 Talents Project’ of

the Chinese Academy of Sciences, the Collaborative Innovation Program of Hefei Science Center, CAS (Grants No. 2020HSC-CIP002), the CASHIPS Director's Fund (BJPY2019B03), the Science Challenge Project under Grant No. TZ2016001, the Major Basic Program of Natural Science Foundation of Shandong Province (Grant No. ZR2021ZD01). A portion of this work was supported by the High Magnetic Field Laboratory of Anhui Province, China.

* Electronic address: zhangping@iapcm.ac.cn

† Electronic address: haon@hmfl.ac.cn

[1] L. Yu, Bound state in superconductors with paramagnetic impurities, *Acta Phys. Sin.* **21**, 75–91 (1965).

[2] H. Shiba, Classical spins in superconductors. *Prog. Theor. Phys.* **40**, 435–451 (1968).

[3] A. I. Rusinov and P. M. Z. E. T. Fiz, On the theory of gapless superconductivity in alloys containing paramagnetic impurities, *JETP Lett.* **9**, 1101–1106 (1968).

[4] J. Kondo, Resistance minimum in dilute magnetic alloys, *Prog. Theor. Phys.* **32**, 37 (1964).

[5] A. V. Balatsky, I. Vekhter, and Jian-Xin Zhu, Impurity-induced states in conventional and unconventional superconductors, *Re. Mod. Phys.* **78**, 373–433 (2006).

[6] J.-X. Yin, Z. Wu, J.-H. Wang, Z.-Y. Ye, J. Gong, X.-Y. Hou, L. Shan, A. Li, X.-J. Liang, X.-X. Wu, J. Li, C.-S. Ting, Z.-Q. Wang, J.-P. Hu, P.-H. Hor, H. Ding and S. H. Pan, Observation of a robust zero-energy bound state in iron-based superconductor Fe(Te,Se), *Nat. Phys.* **11**, 543 (2015).

[7] C. Liu, C. Chen, X. Liu, Z. Wang, Y. Liu, S. Ye, Z. Wang, J. Hu and Jian Wang, Zero-energy bound states in the high-temperature superconductors at the two-dimensional limit, *Sci. Adv.* **6**, eaax7547 (2020).

[8] P. Fan, F. Yang, G. Qian, H. Chen, Y.-Y. Zhang, G. Li, Z. Huang, Y. Xing, L. Kong, W. Liu, K. Jiang, C. Shen, S. Du, J. Schneeloch, R. Zhong, G. Gu, Z. Wang, H. Ding and H.-J. Gao, Observation of magnetic adatom-induced Majorana vortex and its hybridization with field-induced Majorana vortex in an iron-based superconductor, *Nat. Commun.* **12**, 1348 (2021).

[9] D. Wang, J. Wiebe, R. Zhong, G. Gu, and R. Wiesendanger, Spin-Polarized Yu-Shiba-Rusinov States in an Iron-Based Superconductor, *Phys. Rev. Lett.* **126**, 076802 (2021).

[10] D. Chatzopoulos, D. Cho, K. M. Bastiaans, G. O. Steffensen, D. Bouwmeester, A. Akbari, G. Gu, J. Paaske, B. M. Andersen and M. P. Allan, Spatially dispersing Yu-Shiba-Rusinov states in the unconventional superconductor $\text{FeTe}_{0.55}\text{Se}_{0.45}$, *Nat. Commun.* **12**, 298 (2021).

[11] K. Jiang, X. Dai, and Z. Wang, Quantum Anomalous Vortex and Majorana Zero Mode in Iron-Based Superconductor Fe(Te,Se), *Phys. Rev. X* **9**, 011033 (2019).

[12] C.-K. Chiu, Z. Wang, Yu-Shiba-Rusinov states in a superconductor with topological Z_2 bands, *arXiv:2109.15227* (2021).

[13] V. Thampy, J. Kang, J. A. Rodriguez-Rivera, W. Bao, A. T. Savici, J. Hu, T. J. Liu, B. Qian, D. Fobes, Z. Q. Mao, C. B. Fu, W. C. Chen, Q. Ye, R. W. Erwin, T. R. Gentile, Z. Tesanovic, and C. Broholm, Friedel-Like Oscillations from Interstitial Iron in Superconducting $\text{Fe}_{1+y}\text{Te}_{0.62}\text{Se}_{0.38}$, *Phys. Rev. Lett.* **108**, 107002 (2012).

[14] M. E. Flatté and J. M. Byers, Local Electronic Structure of a Single Magnetic Impurity in a Superconductor, *Phys. Rev. Lett.* **78**, 3761 (2012).

[15] R. Kümmel, Electronic Structure of Superconductors with Dilute Magnetic Impurities, *Phys. Rev. B* **6**, 2617 (1972).

[16] A. Yazdani, B. A. Jones, C. P. Lutz, M. F. Crommie, and D. M. Eigler, Probing the Local Effects of Magnetic Impurities on Superconductivity, *Science*, **275** (5307) (1997).

[17] M. I. Salkola, A. V. Balatsky, and J. R. Schrieffer, Spectral properties of quasiparticle excitations induced by magnetic moments in superconductors, *Phys. Rev. B* **55**, 12648 (1997).

[18] T. Meng, J. Klinovaja, S. Hoffman, P. Simon, and D. Loss, Superconducting gap renormalization around two magnetic impurities: From Shiba to Andreev bound states, *Phys. Rev. B* **92**, 064503 (2015).

[19] N. Hao and J. Hu, Topological Phases in the Single-Layer FeSe. *Phys. Rev. X* **4**, 031053 (2014).

[20] Z. Wang, P. Zhang, G. Xu, L. K. Zeng, H. Miao, X. Xu, T. Qian, H. Weng, P. Richard, A. V. Fedorov, H. Ding, X. Dai, and Z. Fang, Topological nature of the $\text{FeSe}_{0.5}\text{Te}_{0.5}$ superconductor. *Phys. Rev. B* **92**, 115119 (2015).

[21] X. Wu, S. Qin, Y. Liang, H. Fan, and J. Hu, Topological characters in $\text{Fe}(\text{Te}_{1-x}\text{Se}_x)$ thin films. *Phys. Rev. B* **93**, 115129 (2016).

[22] G. Xu, B. Lian, P. Tang, X.-L. Qi, and S.-C. Zhang, Topological Superconductivity on the Surface of Fe-Based Superconductors. *Phys. Rev. Lett.* **117**, 047001 (2016).

[23] N. Hao and J. Hu, Topological quantum states of matter in iron-based superconductors: from concept to material realization. *Natl. Sci. Rev.* **6**, 213 (2019).

[24] L. Fu and C. L. Kane, Superconducting Proximity Effect and Majorana Fermions at the Surface of a Topological Insulator, *Phys. Rev. Lett.* **100**, 096407 (2008).

[25] R. Song, P. Zhang and N. Hao, Phase-Manipulation-Induced Majorana Mode and Braiding Realization in Iron-Based Superconductor Fe(Te,Se), *Phys. Rev. Lett.* **128**, 016402 (2022).

[26] J. R. Colbert and P. A. Lee, Proposal to measure the quasiparticle poisoning time of Majorana bound states, *Phys. Rev. B* **89**, 140505(R) (2014).

[27] D. Wang, L. Kong, P. Fan, H. Chen, S. Zhu, W. Liu, L. Cao, Y. Sun, S. Du, J. Schneeloch, R. Zhong, G. Gu, L. Fu, H. Ding, H.-J. Gao, *Science*, **362**, 333–335 (2018).

[28] S. S. Zhang, J.-X. Yin, G. Dai, L. Zhao, T.-R. Chang, N. Shumiya, K. Jiang, H. Zheng, G. Bian, D. Multer, M. Litskevich, G. Chang, I. Belopolski, T. A. Cochran, X. Wu, D. Wu, J. Luo, G. Chen, H. Lin, F.-C. Chou, X. Wang, C. Jin, R. Sankar, Z. Wang, and M. Z. Hasan, *Phys. Rev. B* **101**, 100507(R) (2020).

[29] Z. P. Yin, K. Haule, G. Kotliar, Kinetic frustration and the nature of the magnetic and paramagnetic states in iron pnictides and iron chalcogenides, *Nat. Mater.* **10**, 932–935 (2011).

[30] T. Choi, W. Paul, S. Rolf-Pissarczyk, A. J. Macdonald, F. D. Natterer, K. Yang, P. Willke, C. P. Lutz, and A. J. Heinrich, Atomic-scale sensing of the magnetic dipolar field from single atoms, *Nat. Nanotechnol.* **12**, 420

(2017).

[31] T.g Choi, C. P. Lutz, A. J. Heinrich, Studies of magnetic dipolar interaction between individual atoms using ESR-STM, *Current Applied Physics*, **17**, 11, (2017).

THE CALCULATIONS OF DENSITY FUNCTIONAL THEORY METHODS

The first-principles calculations were performed by density functional theory (DFT) using the Vienna ab initio simulation package (VASP) [1, 2]. The plane-wave basis with an energy cutoff of 350 eV was adopted. The electron-ion interactions were modeled by the projector augmented wave potential (PAW) [3] and the exchange-correlation functional was approximated by the Perdew-Burke-Ernzerhof-type (PBE) generalized gradient approximation (GGA) [4]. Here we use the parameter "I-CONSTRAINED-M" in VASP to constrain the direction of the Fe impurity always along the z axis and give the substrate a very weak magnetic background. As shown in Fig. 4, the differential charge density can reflect the coupling between the impurity and substrate, as the height increases, the chemical adsorption will turn into physical adsorption. To estimate the value of $J(r, z)$, we can set the impurity having a FM and AFM coupling with its nearest iron atoms respectively. And using a simple Heisenberg Hamiltonian, we can calculate the strength of exchange coupling. The local Hamiltonian reads

$$H_M = -J_H \sum_{NN} S_{imp} \cdot S_{NN}, \quad (6)$$

where S_{imp} and S_{NN} is the magnetic moment of the impurity and its nearest neighbor iron atoms. Because the impurity has four nearest neighbor, we can get

$$\Delta E = H_{AFM} - H_{FM} = 8J_H S_{imp} S_{NN}. \quad (7)$$

The effective magnetic field generated by the impurity is

$$h_{imp} = \frac{n \langle S_{imp} \rangle}{\mu_B} \int J_H(r) d\mathbf{r} \quad (8)$$

where n , S_{imp} , μ_B labels the concentration of localized moments, the average value of the localized spins, Bohr magneton and ferromagnetic exchange integral, respectively [5]. For a single impurity, we have $n = 1$ and $J_H(r) = J_H \delta(r)$. The coupling Hamiltonian is

$$H_{coup} = \int d\mathbf{r} J(\mathbf{r}, z_0) \mathbf{S}_{imp} \cdot \boldsymbol{\sigma} \quad (9)$$

The exchange interaction is very local, so we can assume that $J(\mathbf{r}, z_0) = J\delta(r)$, and then we can adopt a mean-field approximation as

$$H_{coup} = \langle JS_{imp} \rangle \sum_{\sigma} \sigma c_{i_0}^{\dagger} c_{i_0}. \quad (10)$$

Comparing Eq. 10 and Eq. 8, we find that the existence of the magnetic impurity is equivalent to applying a local magnetic field at the impurity site. So the strength of the exchange coupling can be characterized by the effective magnetic field generated by the impurity, which can be calculated as

$$\langle JS_{imp} \rangle = \frac{\Delta E}{8S_{NN}} \quad (11)$$

In our calculations, the S_{NN} is set to be $0.05\mu_B$, $S_{imp} = \pm 3\mu_B$ for FM and AFM coupling respectively.

BDG NUMERIC CALCULATIONS IN LATTICE MODEL

We consider a square lattice, the Hamiltonian can be expressed as

$$H_0 = - \sum_i \mu c_i^{\dagger} c_i + \sum_{\langle i,j \rangle} t_{ij} c_i^{\dagger} c_j \quad (12)$$

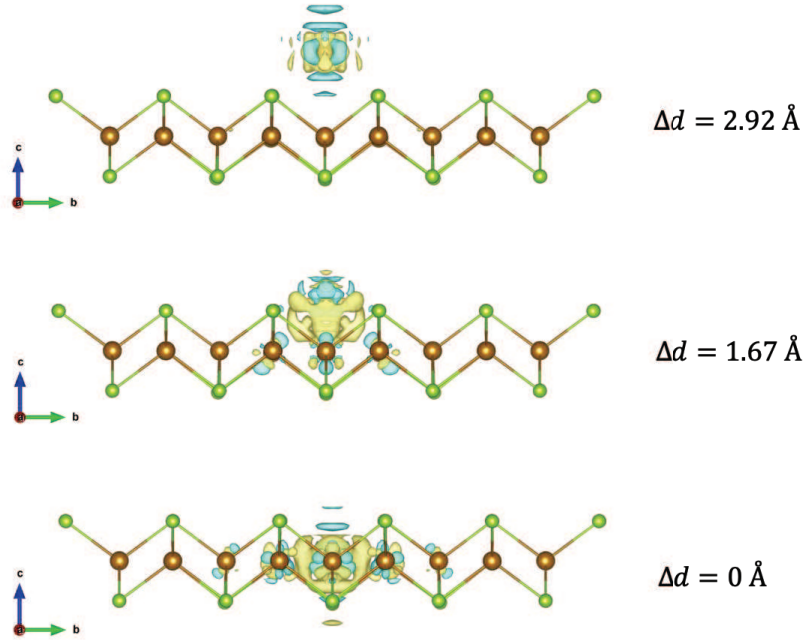


FIG. 4: Differential charge density of different height (a) 2.92 \AA , (b) 1.67 \AA and (c) 0 \AA .

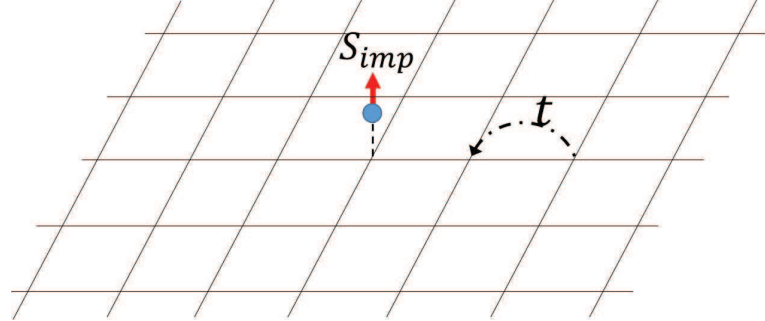


FIG. 5: Scheme of the lattice model.

which includes the on-site term, and nearest-neighbor hopping term. Now a magnetic impurity is put onto the site i_0 and thus would introduce an exchange term as

$$H_{imp} = -J(c_{i_0\uparrow}^\dagger c_{i_0\uparrow} - c_{i_0\downarrow}^\dagger c_{i_0\downarrow}), \quad (13)$$

which performs like an effective magnetic field generated by the impurity. Note that S_{imp} is merged into J for simplicity. And when superconductivity is induced, the Cooper pairing potential is introduced as

$$H_\Delta = \sum_i (\Delta c_{i\uparrow}^\dagger c_{i\downarrow}^\dagger + h.c.) \quad (14)$$

The total Hamiltonian is

$$H = H_0 + H_{imp} + H_\Delta \quad (15)$$

We can perform the Bogoliubov transformation

$$c_{i\sigma} = \sum_n' (u_{i\sigma}^n \gamma_n - \sigma v_{i\sigma}^{n*} \gamma_n^\dagger) \quad (16)$$

where ' denotes summation over the positive eigenvalues, and numerically solve the equations

$$\sum_j \hat{H}_{ij} \phi_j = E_n \phi_i \quad (17)$$

in the Nambu spinor representation $\phi_i = (u_{i\uparrow}^n, u_{i\downarrow}^n, v_{i\uparrow}^n, v_{i\downarrow}^n)^T$ [6]. The matrix elements read

$$\hat{H}_{ij} = \begin{pmatrix} \tilde{t}_{ij\uparrow} & 0 & 0 & \Delta_i \\ 0 & \tilde{t}_{ij\downarrow} & \Delta_i & 0 \\ 0 & \Delta_i & -(\tilde{t}_{ij\uparrow})^* & 0 \\ \Delta_i & 0 & 0 & -(\tilde{t}_{ij\downarrow})^* \end{pmatrix}, \quad (18)$$

where $\tilde{t}_{ij\sigma} = t_j \delta_{\langle ij \rangle} - (\mu + \sigma J \delta_{ii_0}) \delta_{ij}$. And the order parameter Δ_i should be self-consistently determined as

$$\Delta_i(T) = \frac{g}{2} \sum_n' (u_{i\uparrow}^n v_{i\downarrow}^{n*} + u_{i\downarrow}^n v_{i\uparrow}^{n*}) \tanh\left(\frac{E_n}{k_B T}\right) \quad (19)$$

To get the numerical results, we have adopted a 25×25 lattice. The hopping parameter $t = 10 \text{ meV}$, homogeneous order parameter $\Delta_0 = 2 \text{ meV}$ and chemical potential $\mu = 0.1t$.

SOLUTION OF MAJORANA ZERO MODE

Analytic solution

The Hamiltonian of a magnetic field applied to a superconductor with a Dirac-type topological surface state can be expressed as $H = \int d^2r \Psi^\dagger(r) \mathcal{H} \Psi(r)$, where

$$\mathcal{H} = [v_F(k_x \sigma_y - k_y \sigma_x) - \mu] \tau_z + \alpha \sigma \cdot \mathbf{B} + Re(\Delta) \tau_x - Im(\Delta) \tau_y. \quad (20)$$

Here $\Psi = (c_\uparrow, c_\downarrow, c_\downarrow^\dagger, -c_\uparrow^\dagger)$ denotes the Nambu basis, σ_i and τ_i ($i = x, y, z$) are Pauli matrices but spans spin and Nambu space respectively. $\mathbf{B}(\mathbf{r})$ is the external magnetic field $\mathbf{B} = (B_x, B_y, B_z)$. Due to the existence of impurity, translation invariance is broken. Thus we need to solve Eq. (1) in real space with cylindrical coordinate system, and we have following transformation:

$$\begin{aligned} k_x - ik_y &= -ie^{-i\theta} \partial_r - \frac{e^{-i\theta}}{r} \partial_\theta \\ k_x + ik_y &= -ie^{i\theta} \partial_r + \frac{e^{i\theta}}{r} \partial_\theta \end{aligned}$$

Substituting it into Eq. 20, we get the complete form BdG Hamiltonian as

$$\begin{pmatrix} \alpha B_z - \mu & -e^{-i\theta} v_F (\partial_r - \frac{i}{r} \partial_\theta) & \Delta(r) & 0 \\ e^{i\theta} v_F (\partial_r + \frac{i}{r} \partial_\theta) & -\alpha B_z - \mu & 0 & \Delta(r) \\ \Delta(r) & 0 & \alpha B_z + \mu & e^{-i\theta} v_F (\partial_r - \frac{i}{r} \partial_\theta) \\ 0 & \Delta(r) & -e^{i\theta} v_F (\partial_r + \frac{i}{r} \partial_\theta) & -\alpha B_z + \mu \end{pmatrix}. \quad (21)$$

Here, we assume the magnetic field is along the z direction. The BdG equation is

$$\mathcal{H} \psi(r, \theta) = E \psi(r, \theta). \quad (22)$$

Assuming the trivial wave function has the form

$$\psi(r, \theta) = e^{il\theta} \begin{pmatrix} e^{-i\theta/2} u_\uparrow(r) \\ e^{i\theta/2} u_\downarrow(r) \\ e^{-i\theta/2} v_\downarrow(r) \\ -e^{i\theta/2} v_\uparrow(r) \end{pmatrix}$$

Then we can obtain the radial equation of Eq. 22 as:

$$(\alpha B_z - \mu)u_\uparrow(r) - v_F(\partial_r + \frac{l + \frac{1}{2}}{r})u_\downarrow(r) + \Delta(r)v_\downarrow(r) = Eu_\uparrow(r) \quad (23)$$

$$v_F(\partial_r - \frac{l - \frac{1}{2}}{r})u_\uparrow(r) - [\alpha B_z + \mu]u_\downarrow(r) - \Delta(r)v_\uparrow(r) = Eu_\downarrow(r) \quad (24)$$

$$\Delta(r)u_\uparrow(r) + (\alpha B_z + \mu)v_\downarrow(r) - v_F(\partial_r + \frac{l + \frac{1}{2}}{r})v_\uparrow(r) = -Ev_\downarrow(r) \quad (25)$$

$$\Delta(r)u_\downarrow(r) - v_F(\partial_r - \frac{l - \frac{1}{2}}{r})v_\downarrow(r) + (\alpha B_z - \mu)v_\uparrow(r) = -Ev_\uparrow(r) \quad (26)$$

The matrix form is :

$$\begin{pmatrix} \alpha B_z - \mu & -v_F(\partial_r + \frac{\nu+1}{r}) & \Delta(r) & 0 \\ v_F(\partial_r - \frac{\nu}{r}) & -\alpha B_z - \mu & 0 & \Delta(r) \\ \Delta(r) & 0 & \alpha B_z + \mu & v_F(\partial_r + \frac{\nu+1}{r}) \\ 0 & \Delta(r) & -v_F(\partial_r - \frac{\nu}{r}) & -\alpha B_z + \mu \end{pmatrix}, \quad (27)$$

where $\nu = l - \frac{1}{2}$.

And the Majorana solution requests $\mathcal{C}\psi(r, \theta) = \eta\psi(r, \theta)$, where the particle-hole operator $\mathcal{C} = \tau_y\sigma_y K$, with K the complex conjugation operator, and η is some constant. Without loss of generality, we assume $u_{\uparrow(\downarrow)}(r)$ and $v_{\uparrow(\downarrow)}(r)$ is real. This yields the following constraint condition:

$$u_\uparrow(r) = \eta v_\uparrow(r) \quad (28)$$

$$u_\downarrow(r) = \eta v_\downarrow(r) \quad (29)$$

$$l = 0 \quad (30)$$

Obviously, η can only be $+1$ or -1 , and they correspond to the exponential increase and decay solution, respectively. For an infinite large 2D space, only $\eta = -1$ is reasonable. And then the equation set of Eqs. 23, 24, 25, 26 can be reduced as

$$(\alpha B_z - \mu)u_\uparrow(r) - \left[v_F(\partial_r + \frac{1}{2r}) + \Delta(r) \right] u_\downarrow(r) = Eu_\uparrow(r) \quad (31)$$

$$\left[v_F(\partial_r + \frac{1}{2r}) + \Delta(r) \right] u_\uparrow(r) - [\alpha B_z + \mu]u_\downarrow(r) = Eu_\downarrow(r) \quad (32)$$

, for the Majorana condition we can set $E = 0$.

Now, let's check the simplest condition where $B_z = 0$, which means there is no magnetic effect and then the system should return to the TI+SC model, however with a antiperiodic boundary condition $\psi(r, \theta) = -\psi(r, \theta + 2\pi)$. When $B_z = 0$, Eq. (12) and (13) can be reduced to :

$$u_{\uparrow(\downarrow)}''(r) + \frac{u_{\uparrow(\downarrow)}'(r)}{r} + \left(\frac{\mu^2 + \Delta_0^2}{v_F^2} - \frac{1}{4r^2} \right) u_{\uparrow(\downarrow)}(r) + \frac{2\Delta_0}{v_F} \left[u_{\uparrow(\downarrow)}'(r) + \frac{1}{2r} u_{\uparrow(\downarrow)}(r) \right] = 0 \quad (33)$$

The solution of $u_\uparrow(r)$ is

$$u_\uparrow(r) = c_1 \frac{e^{-ik_F r}}{\sqrt{r}} e^{-r/\xi_0} + c_2 \frac{e^{ik_F r}}{\sqrt{r}} e^{-r/\xi_0} \quad (34)$$

$$u_\downarrow(r) = -i(c_1 \frac{e^{-ik_F r}}{\sqrt{r}} - c_2 \frac{e^{ik_F r}}{\sqrt{r}}) e^{-r/\xi_0} \quad (35)$$

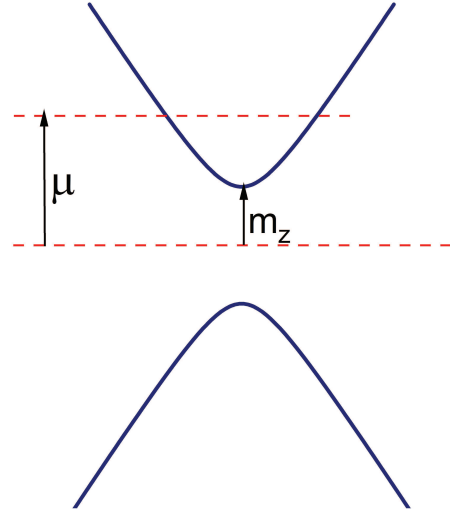


FIG. 6: TI with a z-direction magnetic field. Only when $\mu > m_z$ there exists a spin-momentum-locked fermi surface and it is topological nontrivial.

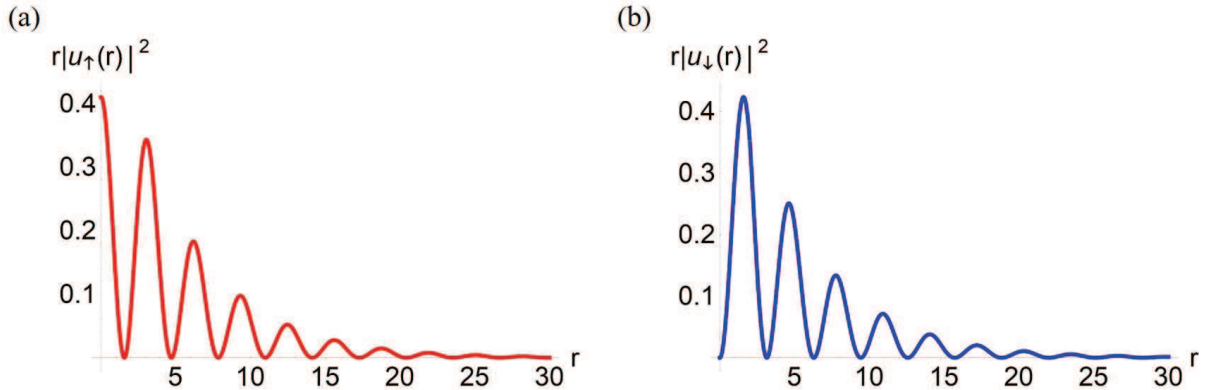


FIG. 7: Wave functions of analytic solution.

where $\xi_0 = \frac{v_F}{\Delta_0}$, $k_F = \frac{\mu}{v_F}$. Note that c_1 should equal to c_2 to ensure $u(r)$ is real, and then the radial wave functions can be reduced as $u_{\uparrow/\downarrow}(r) \propto J_{\mp 1/2}(k_F r) e^{-r/\xi_0}$, by contrast with the vortex condition the order of Bessel function has a $\frac{1}{2}$ shift. And if $B_z \neq 0$, we set $m_z = \alpha B_z$, the parameter k_F is modified as $k_F = \frac{\sqrt{\mu^2 - m_z^2}}{v_F}$. It is easy to find that if $|m_z| > |\mu|$ the wave function is divergent when $r \rightarrow \infty$. Actually, only when $\mu > m_z$ it's topological nontrivial. So the key point to get Majorana zero-energy mode is the antiperiodic boundary condition, $\psi(r, \theta) = -\psi(r, \theta + 2\pi)$.

Quasiparticle scattering

From Eq. (34) and (35), it's easy to find that the wave functions of Majorana modes can always be divided into two parts according to its radial propagating directions, *i.e.* towards or dorsad the impurity center. We define $e^{-ik_F r}$ as a converging wave. Here the scattering effect caused by the impurity should be considered. In a 2D space where the rotation symmetry is preserved, the scattering wave function should be described by the cylindrical wave. The scattering process can be understood as Fig. 8, we name the wave functions of incoming and scattering as ψ_{in} and

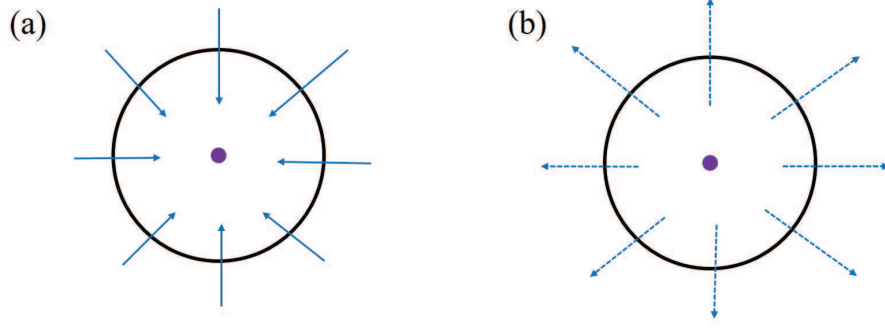


FIG. 8: (a) The converging cylindrical wave propagates to the impurity and (b) is scattered into a diverging cylindrical wave.

ψ_s , respectively, their specific form is :

$$\psi_{in} = C \frac{e^{-ik_F r}}{\sqrt{r}} e^{r/\xi_0} \quad (r < R_0) \quad (36)$$

$$\psi_s = f(\theta) \frac{e^{ikr}}{\sqrt{r}}, \quad (37)$$

where $f(\theta)$ is the scattering amplitude, and the scattering interface is defined as $\sigma(\theta) = |f(\theta)|^2$ [7]. The incoming and scattering current density can be defined by the following formula

$$j = \frac{i\hbar}{2m} (\psi \nabla \psi^* - \psi^* \nabla \psi). \quad (38)$$

So the specific expression of the scattering wave function should be solved from the flow conservation and Schrödinger equation :

$$j_{in} = j_s \quad (39)$$

$$\frac{\hbar^2}{2m} \nabla^2 \psi_s + U(r) \psi_s = E \psi_s \quad (40)$$

where $U(r)$ is the scattering potential, for a single impurity we can consider it as a local potential $U(r) = U_0 \delta(r)$, and the elastic scattering requests $E = 0$ since the scattered particle is Majorana fermion. According to the method of partial, we can decompose the scattering wave function into different angular-momentum channel by using

$$e^{ikr \cos \theta} = J_0(kr) + \sum_{n=1}^{\infty} i^n J_n(kr) \cos n\theta \quad (41)$$

It is known that for a local δ potential, only s wave i.e. $l = 0$ is involved, so it's obvious to simplify the scattering wave function as $\psi_s(r, \theta) = f(\theta) J_0(kr) / \sqrt{r}$. Thus the additional density of states (DOS) at zero energy caused by the elastic scattering is

$$N_s(E = 0, r, \theta) \propto r |\psi_s(r, \theta)|^2 \propto J_0^2(kr). \quad (42)$$

Here $|f(\theta)|$ is approximated to a constant because $\int_0^{2\pi} f(\theta) d\theta = \text{constant}$. Considering this modulation about zero-energy DOS, we obtain

$$N(E = 0, r) = N_s^0 J_0^2(kr) + N_M^0(r) \quad (43)$$

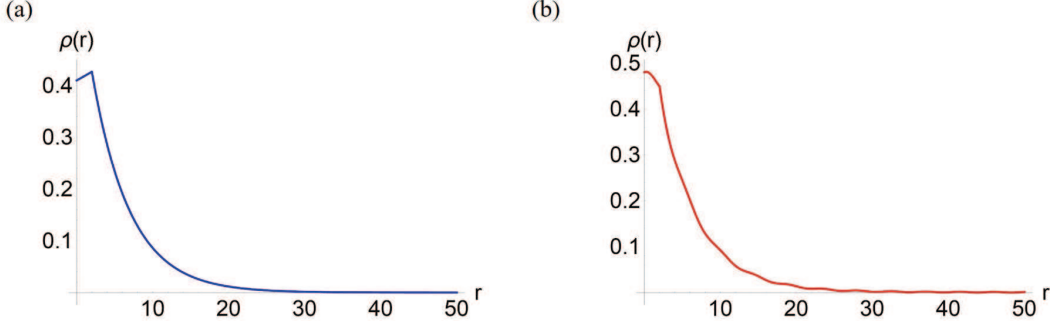


FIG. 9: Probability density (a) before and (b) after taking into account of the quasiparticle-scattering effect, the former is a simple summation of spin-up and spin-down part in Fig. 7 and the latter include the scattering wave functions.

Numerical Solution

Now we use Bessel functions as a complete orthogonal base to expand the wave function [8]. That is

$$u_{\uparrow}(r) = \sum_{n=1}^N u_n^{\uparrow} \varphi_{\nu,n}(r) \quad (44)$$

$$u_{\downarrow}(r) = \sum_{n=1}^N u_n^{\downarrow} \varphi_{\nu+1,n}(r) \quad (45)$$

$$v_{\downarrow}(r) = \sum_{n=1}^N v_n^{\downarrow} \varphi_{\nu+1,n}(r) \quad (46)$$

$$v_{\uparrow}(r) = \sum_{n=1}^N v_n^{\uparrow} \varphi_{\nu,n}(r) \quad (47)$$

$$(48)$$

where $\nu = l - \frac{1}{2}$, $\varphi_{\nu,n} = \frac{\sqrt{2}}{R J_{\nu+1}(j_{\nu,n} \frac{r}{R})} J_{\nu}(j_{\nu,n} \frac{r}{R})$, N is the cutoff number. Then the radial equation Eq. 27 can be reduced as a $4N \times 4N$ matrix and its eigenvalues are the energies. We define:

$$T_{ij}^{\nu} = \alpha \int_0^R B_z \varphi_{\nu,i}(r) \varphi_{\nu,j}(r) r dr \quad (49)$$

$$V_{ij}^{\nu,\nu+1} = v_F \int_0^R r \varphi_{\nu,i}(r) (\partial_r + \frac{\nu+1}{r}) \varphi_{\nu+1,j}(r) dr \quad (50)$$

$$S_{ij}^{\nu+1,\nu} = v_F \int_0^R r \varphi_{\nu+1,i}(r) (\partial_r - \frac{\nu}{r}) \varphi_{\nu,j}(r) dr \quad (51)$$

$$\Delta_{ij}^{\nu} = \int_0^R \Delta(r) \varphi_{\nu,i}(r) \varphi_{\nu,j}(r) r dr \quad (52)$$

Here, the order parameter varies in the space can be approximately calculated as $\Delta(r) = \Delta_0 (1 - \alpha \frac{1 - \cos(2k_F r)}{k_F^2 r^2})$ when $R_0 \ll \xi_0$ and $T \ll T_c$ [9]. Then the eigenvalue equation can be expressed as :

$$Det \begin{pmatrix} T^{\nu} - \mu & -V^{\nu,\nu+1} & \Delta^{\nu} & 0 \\ S^{\nu+1,\nu} & -T^{\nu+1} - \mu & 0 & \Delta^{\nu+1} \\ \Delta^{\nu} & 0 & T^{\nu} + \mu & V^{\nu+1,\nu} \\ 0 & \Delta^{\nu+1} & -S^{\nu,\nu+1} & -T^{\nu+1} + \mu \end{pmatrix} = E \quad (53)$$

To get the numerical results, we have set the radius of the disk as $R = 800 \text{ \AA}$, the Fermi velocity $v_F = 200 \text{ meV \AA}$ as the experimental measurement [10], $\mu = 1 \text{ meV}$ and the cut-off number $N = 50$ which is accurate enough to affirm the Majorana zero-energy mode. The results are shown in Fig. 10.

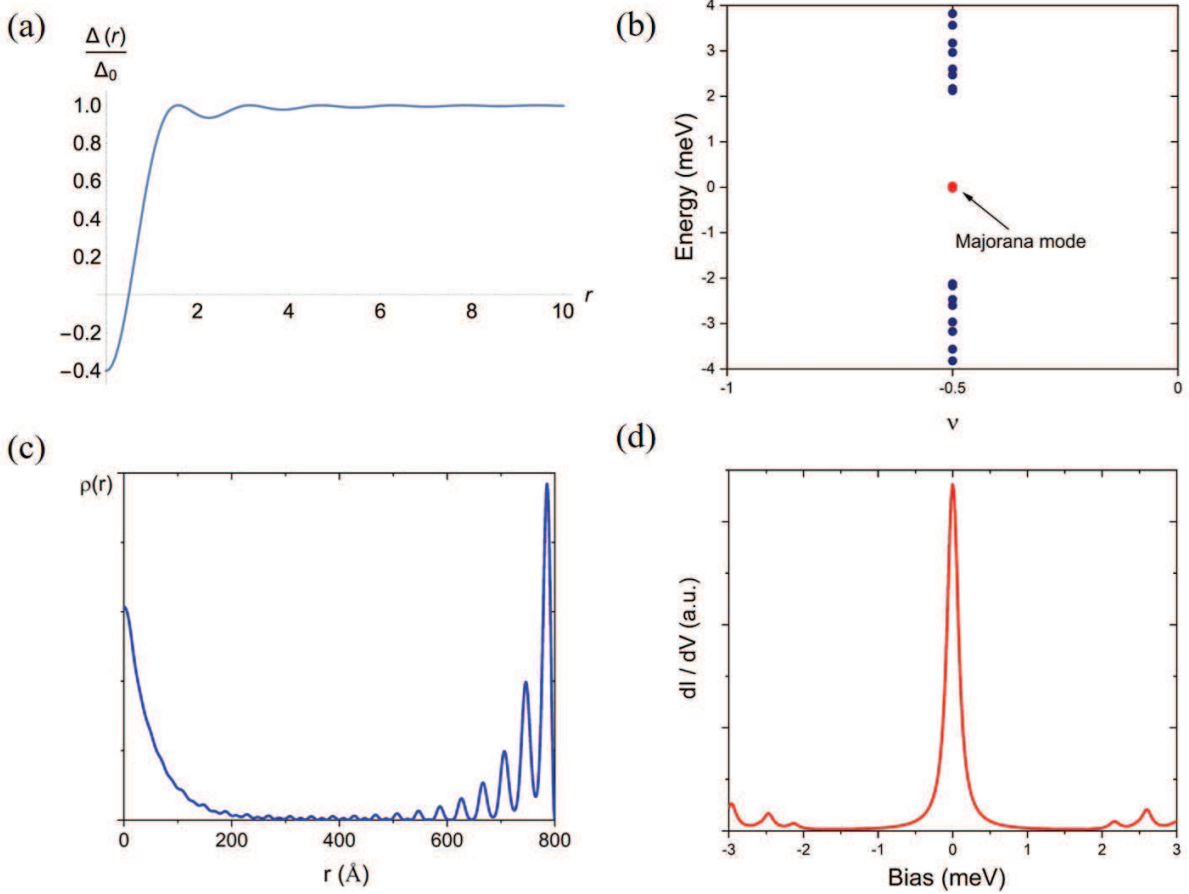


FIG. 10: (a) Variation of order parameter in space; (b) Energy spectrum for $\nu = -\frac{1}{2}$ ($l = 0$); (c) Radial probability density; (d) Simulated STM spectrum at the core $r = 0$.

The Majorana condition requests that $\mathcal{C}\psi = \eta\psi$, in the main text we choose $\eta = -1$ because we adopt a infinite large diameter of the disk and if $\eta = 1$ the wave functions have an exponentially increasing form, which is not physical. However if the diameter is finite, $\eta = 1$ would be reasonable and forms another probability-density peak at the boundary. Thus the zero-energy solution should be a linear combination of $\eta = \pm 1$ as

$$\psi = \sum_{\eta} a_{\eta} \varphi_{\eta}. \quad (54)$$

And that is the reason why every zero-energy mode contains both the core and edge state.

Vortex condition

For comparison, we also analyzed the general vortex-induced Majorana mode. When there exist quantum vortexes, the SC order parameter should have a attached phase as $\Delta = \Delta(r)e^{i\theta}$. The complete Hamiltonian can be expressed as

$$\begin{pmatrix} -\mu & -e^{-i\theta}v_F(\partial_r - \frac{i}{r}\partial_{\theta}) & \Delta(r)e^{i\theta} & 0 \\ e^{i\theta}v_F(\partial_r + \frac{i}{r}\partial_{\theta}) & -\mu & 0 & \Delta(r)e^{i\theta} \\ \Delta(r)e^{-i\theta} & 0 & \mu & e^{-i\theta}v_F(\partial_r - \frac{i}{r}\partial_{\theta}) \\ 0 & \Delta(r)e^{-i\theta} & -e^{i\theta}v_F(\partial_r + \frac{i}{r}\partial_{\theta}) & \mu \end{pmatrix} \quad (55)$$

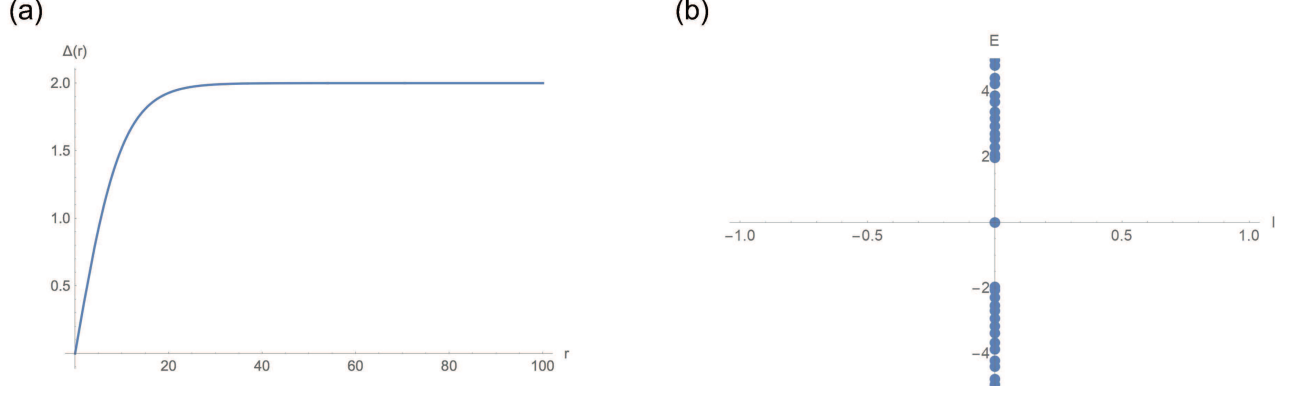


FIG. 11: (a) The order parameter from the core to the edge of a vortex and (b) the energy spectrum of momentum $l = 0$.

Correspondingly, the trivial wave functions should have this form

$$\psi(r, \theta) = e^{il\theta} \begin{pmatrix} u_\uparrow(r) \\ e^{i\theta} u_\downarrow(r) \\ e^{-i\theta} v_\downarrow(r) \\ v_\uparrow(r) \end{pmatrix} \quad (56)$$

Also, the Majorana condition requests that

$$l = 0 \quad (57)$$

$$u_\uparrow(r) = -\eta v_\uparrow(r) \quad (58)$$

$$u_\downarrow(r) = \eta v_\downarrow(r) \quad (59)$$

The radial equation can be obtained as

$$\begin{pmatrix} -\mu & -v_F(\partial_r + \frac{l+1}{r}) & \Delta(r) & 0 \\ v_F(\partial_r - \frac{l}{r}) & -\mu & 0 & \Delta(r) \\ \Delta(r) & 0 & \mu & v_F(\partial_r + \frac{l}{r}) \\ 0 & \Delta(r) & -v_F(\partial_r - \frac{l-1}{r}) & \mu \end{pmatrix} \begin{pmatrix} u_\uparrow(r) \\ u_\downarrow(r) \\ v_\downarrow(r) \\ v_\uparrow(r) \end{pmatrix} = E \begin{pmatrix} u_\uparrow(r) \\ u_\downarrow(r) \\ v_\downarrow(r) \\ v_\uparrow(r) \end{pmatrix} \quad (60)$$

Here, we first derive the analytic solution for Majorana mode when $\Delta(r)$ is approximated as a constant Δ_0 . Similarly, the equation can be simplified as

$$u_\uparrow''(r) + \left(\frac{2}{\xi_0} + \frac{1}{r}\right) u_\uparrow'(r) + \left(\frac{1}{\xi_0^2} + \frac{1}{r\xi_0} + k_F^2\right) u_\uparrow(r) = 0 \quad (61)$$

the solution can be obtained as :

$$u_\uparrow(r) = c_1 J_0(k_F r) e^{-r/\xi_0} \quad (62)$$

$$u_\downarrow(r) = -c_1 J_1(k_F r) e^{-r/\xi_0}, \quad (63)$$

which is consistent with Ref. [11, 12].

Now we will perform the numerical solution of Eq. (60), the method is the same as above. The space variation of order parameter is adopted as $\Delta(r) = \Delta_0 \tanh \frac{r}{\xi_0}$ [13]. The results are shown in Figs. 11 and 12.

* Electronic address: zhangping@iapcm.ac.cn

† Electronic address: haon@hmfl.ac.cn

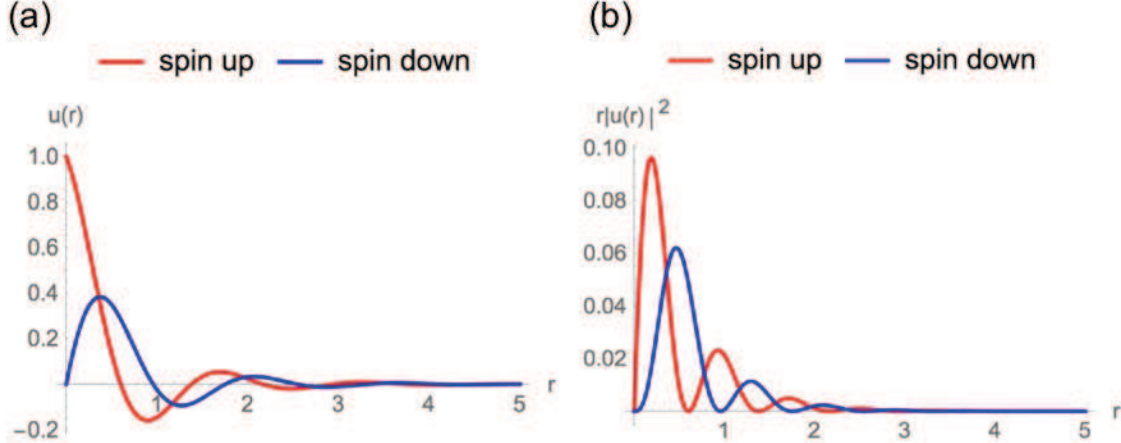


FIG. 12: (a) wave functions and (b) the probability density for the vortex-induced Majorana mode.

- [1] G. Kresse and J. Furthmüller, Efficient iterative schemes for ab initio total-energy calculations using a plane-wave basis set, *Phys. Rev. B* **54**, 11169 (1996).
- [2] G. Kresse and D. Joubert, From ultrasoft pseudopotentials to the projector augmented-wave method, *Phys. Rev. B* **59**, 1758 (1999).
- [3] P. E. Blchl, *Phys. Rev. B* **50**, 17953 (1994).
- [4] J. P. Perdew, K. Burke, and M. Ernzerhof, Projector augmented-wave method, *Phys. Rev. Lett.* **77**, 3865 (1996).
- [5] A. I. Buzdin, Proximity effects in superconductor-ferromagnet heterostructures, *Rev. Mod. Phys.* **77**, 935 (2005).
- [6] Jian-Xin Zhu, Wonkee Kim, C. S. Ting, and J. P. Carbotte, Quasiparticle States around a Nonmagnetic Impurity in a d-Density-Wave State of High- T_c Cuprates, *Phys. Rev. Lett.* **87**, 197001 (2001).
- [7] Sakurai J J, Advanced Quantum Mechanics [M], Addison Wesley, New York, (1967).
- [8] Li Mao and Chuanwei Zhang, Robustness of Majorana modes and minigaps in a spin-orbit-coupled semiconductor-superconductor heterostructure, *Phys. Rev. B* **82**, 174506 (2010).
- [9] Reiner Kümmel, Electronic Structure of Superconductors with Dilute Magnetic Impurities, *Phys. Rev. B* **6**, 2617 (1972).
- [10] D. Wang, L. Kong, P. Fan, H. Chen, S. Zhu, W. Liu, L. Cao, Y. Sun, S. Du, J. Schneeloch, R. Zhong, G. Gu, L. Fu, H. Ding, and H.-J. Gao, Evidence for Majorana bound states in an iron-based superconductor, *Science* **362**, 333 (2018).
- [11] Takuto Kawakami and Xiao Hu, Evolution of Density of States and a Spin-Resolved Checkerboard-Type Pattern Associated with the Majorana Bound State. *Phys. Rev. Lett.* **115**, 177001 (2015).
- [12] Hao-Hua Sun, Kai-Wen Zhang, et al, Majorana Zero Mode Detected with Spin Selective Andreev Reflection in the Vortex of a Topological Superconductor. *Phys. Rev. Lett.* **116**, 257003 (2016).
- [13] François Gygi and Michael Schlüter, Self-consistent electronic structure of a vortex line in a type-II superconductor, *Phys. Rev. B* **43**, 7609 (1991).